

2

5

6

7

8

10

11

13

16

17

18

22

24

26

27



30 **Key Points:**

- 31 • An explainable deep transfer learning framework was developed to predict
32 isoprene concentrations and their variations.
- 33 • Different drivers accounted for historical trends of isoprene concentrations in
34 Hong Kong and London from 1990 to 2023.
- 35 • Reducing nitrogen oxides would alleviate ozone pollution driven by rising
36 temperatures and isoprene levels in the warming climate.
37



38 **Abstract**

39 Isoprene, the globally most abundant volatile organic compound, significantly impacts
40 air quality. Determining isoprene concentration variations and their drivers is a
41 persistent challenge. Here, we developed a robust machine learning framework to
42 simulate isoprene concentrations, without requiring localized emission inventories and
43 explicit chemistry. Temperature, radiation, and surface pressure were the primary
44 drivers of short-term isoprene variations across Chinese cities. On climatic timescales,
45 urban greenspace expansion and climate warming drove isoprene increases by 341 pptv
46 in Hong Kong during 1990–2023, but traffic emission reductions in London
47 counteracted the isoprene rise that climate warming would have otherwise caused (-755
48 pptv vs. +31 pptv). Driven by rising temperatures and isoprene levels, ozone would
49 increase by up to 1.7-fold by 2100 under the high-emission scenario. However,
50 ambitious reduction in nitrogen oxides would alleviate this growth to 1.2-fold. The
51 study has the potential to inform air quality management in a warming climate.

52



53 **1 Introduction**

54 Isoprene is the most abundant non-methane volatile organic compound (VOC) globally,
55 with the total emissions reaching approximately 500 TgC per year, exceeding those of
56 the total anthropogenic VOCs (Guenther et al., 2012; Huang et al., 2017). The high
57 atmospheric reactivity makes it a key precursor for tropospheric ozone (O₃) and
58 secondary organic aerosol, both of which significantly impact air quality and climate
59 (Paulot et al., 2012; Lin et al., 2013). In particular, the effect is pronounced in urban
60 environments due to the interactions between isoprene and anthropogenic emissions
61 (Xu et al., 2015).

62 Terrestrial vegetation is the primary source of atmospheric isoprene, and the emissions
63 are influenced by plant species, geographical locations, and environmental conditions
64 (Guenther et al., 1994; Guenther et al., 1993). Urban landscapes show remarkable
65 diversity in isoprene production, exemplified by stark differences between tree species.
66 While urban greenspace offers numerous benefits, it also emerges as a notable
67 contributor to urban isoprene (Ma et al., 2022). The emissions are highly sensitive to
68 meteorological conditions (Wang et al., 2024a). The combination of climate warming
69 and urbanization lead to intensified urban heat, which in turn boosts isoprene emissions
70 from greenspace (Li et al., 2024; Pfannerstill et al., 2024). In addition, studies have
71 shown that a portion of urban isoprene may stem from motor vehicles, the contribution
72 of which varies by location and season (Borbon et al., 2001). However, vehicle
73 emissions of isoprene do not necessarily increase with growing vehicle population, due
74 to stringent emission controls in many cities. This further complicates the task of
75 accurately simulating the concentrations and trends of urban isoprene. While isoprene
76 may also be emitted from other anthropogenic sources, such as petrochemical activities
77 and coal combustion, the amounts are generally small compared to biogenic emissions,
78 especially in warm seasons (Peron et al., 2024).

79 Modeling and measurement deficiencies remain a serious concern in isoprene research
80 across multiple disciplines. For example, the Model of Emissions of Gases and
81 Aerosols from Nature (MEGAN) estimates vegetation emissions based on theoretical



relationships with meteorology and vegetation dynamics. This model significantly underestimates isoprene emissions from urban greenspace when it is driven by coarse resolution (e.g., >30 m) satellite-derived vegetation data (Ma et al., 2019; Ma et al., 2022). It is also difficult for current chemical transport models to accurately simulate isoprene concentrations, mainly resulting from the grid resolution and uncertainties in isoprene emissions, vertical dispersion rates and oxidation parameterization schemes (Arneth et al., 2011; Guenther et al., 2012). Local vegetation surveys and emission factor measurements can be made to improve model performance. However, the work is challenging and the outcomes often point out additional uncertainties (Seco et al., 2022; Wang et al., 2024b). While isoprene measurements have demonstrated reliability in atmospheric chemistry research, the temporal and spatial coverage remains suboptimal. Given these constraints, there are insufficient robust isoprene data available over climatic timescales (e.g., several decades) to reveal the drivers of long-term trends. To confront this dilemma, we developed a generalized physics-informed neural network based on a residual Multi-Layer Perceptron with a transfer training strategy to reproduce/predict ambient isoprene concentrations. The model was trained by a comprehensive set of isoprene data observed at ten sites in China (a total of ~65,000 hourly data) and validated by a total of ~8,500 hourly and daily data at six overseas sites (Table S1). The model was verified for its ability to predict isoprene with limited sizes of observational data and understand intricate relationships between isoprene and influencing factors. The model was then used to predict future trends of isoprene and the resulting O₃ variations in different climate scenarios. This study enhances our understanding of the responses of ambient isoprene concentrations to emissions and meteorology, and has the potential to inform urban planning and air quality policies in the warming climate.

107



108 2 Data and Models

109 2.1 Isoprene Data and Deep Learning Model

110 A total of over 72,000 hourly (and a small fraction of daily) data of isoprene
 111 concentrations in the daytime (06:00–20:00 local time) of warm seasons (May–October)
 112 were compiled from 16 sites worldwide. Around 88% the data was from different parts
 113 of China, and the remainder was from North America, Amazonia, India, and the UK
 114 (see Table S1). To ensure comparability, we included only online measurements,
 115 excluding offline sampling and analysis methods. While inter-instrument bias might
 116 exist, the isoprene variability within each site was expected to be much larger than any
 117 plausible inter-instrument bias. Moreover, this will not influence the analysis of
 118 isoprene variations at individual sites.

119 The residual multi-layer perceptron architecture (ResMLP) was employed to
 120 approximate the complicated responses of isoprene concentrations to input features,
 121 which was coupled with a physics-informed neural network, thereby PINN-ResMLP.
 122 This approach integrated domain knowledge by enforcing monotonicity constraints
 123 between isoprene and its major sources (e.g., vegetation and traffic emissions), thus
 124 ensuring physically consistent predictions. These constraints were implemented
 125 directly in the model's loss function, which combined terms for data fitting,
 126 monotonicity regularization, and network structure penalties. As a fully data-driven
 127 model, ResMLP may learn patterns that are inconsistent with physical laws.
 128 Incorporating expert knowledge and physical constraints into the model can guide the
 129 learning processes. In this study, we stipulated that isoprene concentrations were
 130 positively correlated with the biogenic and traffic emission sources. This relationship
 131 therefore can be expressed as:

$$132 \quad \frac{\partial ISOP}{\partial VI} > 0 \quad (1)$$

$$133 \quad \frac{\partial ISOP}{\partial BC_{traffic}} > 0 \quad (2)$$



where ISOP represents isoprene concentrations; VI is vegetation index derived from Leaf Area Index (LAI) and Normalized Difference Vegetation Index (NDVI) (see Text S1); and BC_{traffic} is traffic emissions of black carbon. To satisfy this priori knowledge, we developed PINN-ResMLP to constrain the model. The optimization objective of PINN-ResMLP included data item loss ($\mathcal{L}_{\text{data}}$), physical inconsistency loss ($\mathcal{L}_{\text{monotonicity}}$), and additional structural loss ($\mathcal{L}_{\text{structure}}$). Meanwhile, the L2 norm of the network parameters, namely adding the sum of the squares of all network weights (parameters) to the loss function, could effectively regularize and prevent overfitting in PINN-ResMLP. Finally, the total function was formulated as:

$$\mathcal{L} = \mathcal{L}_{\text{data}} + \alpha \cdot \mathcal{L}_{\text{monotonicity}} + \beta \cdot \mathcal{L}_{\text{structure}} \quad (3)$$

$$\mathcal{L}_{\text{data}} = \frac{1}{2N} \sum_{i=1}^N \left[(ISOP_{\text{obs},i} - ISOP_{\text{pred},i})^2 + |ISOP_{\text{obs},i} - ISOP_{\text{pred},i}| \right] \quad (4)$$

$$\mathcal{L}_{\text{monotonicity}} = \frac{1}{N} \sum_{i=1}^N \left[1 - \frac{\text{sign}\left(\frac{\partial ISOP}{\partial VI}\right) + \text{sign}\left(\frac{\partial ISOP}{\partial BC_{\text{traffic}}}\right)}{2} \right] \quad (5)$$

$$\text{sign}(\theta) = \begin{cases} -1, & \theta < 0 \\ 1, & \theta \geq 0 \end{cases} \quad (6)$$

$$\mathcal{L}_{\text{structure}} = \sum_{i=1}^M (W_i^2 + b_i^2) \quad (7)$$

where the α and β are trade-off parameters; N is the number of training samples; i represents a certain sample; $ISOP_{\text{obs}}$ and $ISOP_{\text{pred}}$ are observed and predicted isoprene concentrations, respectively; M is the number of layers in PINN-ResMLP.

Predictor variables were selected to capture key sources and sinks of isoprene, including VI (see Text S1), meteorological parameters (e.g., temperature, solar radiation), and black carbon emitted from traffic (BC_{traffic}) as a proxy for anthropogenic emissions. Full variable definitions and sources are provided in Table S2.

To address data scarcity at some sites, we implemented a supervised transfer learning strategy. The PINN-ResMLP was pre-trained on data-rich sites and fine-tuned with limited data from target sites (see Table S3). Three training strategies were adopted: (1) transfer learning (T), where models were pre-trained on data from other sites and fine-



159 tuned on the target site; (2) no-transfer (NT), where models were trained solely on target
160 site data; and (3) mixed training (MIX) using combined data from all sites. Model
161 performance was evaluated using four-fold cross-validation (Table S3) and metrics
162 including normalized mean absolute error (NMAE) and R^2 . Comparisons were made
163 against standard machine learning algorithms, such as Random Forest (RF), extreme
164 gradient boosting (XGB), and support vector machine (SVM). All algorithms were
165 optimized using extensive grid search (see hyperparameters in Table S4).

166 **2.2 Attribution of Long-term Isoprene Trends and O₃ Projections**

167 The PINN-ResMLP model was also used to quantify the contributions of different
168 factors to the long-term trends of isoprene concentrations at three sites in Hong Kong
169 and London using a scenario-based approach. Using the historical data of
170 meteorological parameters, VI and BC_{traffic} as the input of the PINN-ResMLP_T model,
171 we predicted the summertime (June to August) isoprene concentrations in Hong Kong
172 and London for the period of 1990–2023 (base scenario). In order to reveal the impacts
173 of the major drivers on the isoprene variations, we also predicted the isoprene
174 concentrations by fixing the temperature, VI and BC_{traffic} as their averages over the
175 above period one by one (controlled scenarios). The differences in the predicted
176 isoprene ($\text{isoprene}_{\text{diff}}$) between the base and controlled scenarios depicted the isoprene
177 trends induced by the individual factors. The $\text{isoprene}_{\text{diff}}$ was then compared between
178 different time periods, e.g., the first and last 17 years and the first, middle and last
179 decades. Besides, the coefficient of variation (CV) was calculated for the predicted
180 isoprene concentrations in all the scenarios over the period of 1990–2023. The CV
181 differences between the base and controlled scenarios indicate how the changes in
182 temperature, VI and traffic emissions (represented by BC_{traffic}) increased or decreased
183 the variations in isoprene concentrations.

184 Additionally, future isoprene concentrations at the Hong Kong site were projected for
185 2030–2100 based on temperature changes under different climate scenarios developed
186 by the Coupled Model Intercomparison Project Phase 6 (CMIP6), while keeping other
187 influencing factors constant. Briefly, we used the temperature data from four Shared



188 Socioeconomic Pathways (SSPs), including SSP126 (low forcing), SSP245
189 (intermediate forcing), SSP370 (medium-high forcing), and SSP585 (high forcing), and
190 held the other influencing factors constant. The averages of outputs from four Coupled
191 Model Intercomparison Project Phase 6 (CMIP6) models (ACCESS-CM2, CMCC-
192 ESM2, MPI-ESM1-2-HR, and GFDL-ESM4) were adopted (Xu et al., 2024).

193 Using the future profiles of temperature and isoprene as constraints, we simulated O₃
194 concentrations as a function of isoprene and temperature using a zero-dimensional box
195 model under different NO_x reduction scenarios. The Framework for 0-D Atmospheric
196 Modeling (F0AM) incorporating Master Chemical Mechanism v3.3.1 was used to
197 simulate O₃ under different sets of temperatures and isoprene concentrations (Lyu et al.,
198 2024). The model was constrained by the average diurnal profiles of air pollutants
199 (excluding O₃) and meteorological parameters observed in the summer of 2023 at the
200 Hong Kong_TC site, except that the daytime average temperature changed from 22 °C
201 to 38 °C in 2 °C intervals and the daytime average isoprene concentrations varied in the
202 range of 0.15–1.8 ppbv in intervals of 0.15 ppbv. The O₃ isopleths were depicted using
203 the simulation results for 108 temperature-isoprene settings. Additionally, the above
204 simulations were repeated in different scenarios of NO_x reduction, i.e., 49.7% and 82.6%
205 under the SSP370 and SSP126, respectively. It is worth noting that the diurnal profiles
206 of other O₃ precursors, such as VOCs and carbon monoxide, were kept unchanged
207 throughout all the simulations.

208



209 **3 Results and Discussion**

210 **3.1 Simulating Isoprene Concentrations Using PINN-ResMLP_T Model**

211 The isoprene concentrations averaged over the respective observation periods varied
212 significantly from 0.15 ppbv in Wuhan to 2.79 ppbv in New Delhi (Figure 1 and Figure
213 S1), due to the differences in sampling periods, climatic conditions, and vegetation type
214 and density. We noticed that most cities have experienced an increase in greenspace in
215 the last 20 years, and there existed significant differences in greenspace coverage and
216 its recent trends between the cities (e.g., Hong Kong versus London). The high
217 vegetation cover appeared to explain the elevated levels of isoprene in South China and
218 Amazonia. Temperature also had a strong effect on isoprene concentrations, as
219 indicated by the Pearson correlation coefficient (R) between hourly isoprene and
220 temperature at individual sites, i.e., 0.41–0.72. The temperature and temperature
221 variation were spatially non-uniform, implying its inconsistent roles in affecting
222 biogenic isoprene emissions. Additionally, anthropogenic emissions might have made
223 significant contributions to isoprene in New Delhi, given the high nocturnal levels and
224 the peak in evening rush hours (Figure S2). This was also mentioned in a previous study
225 (Tripathi et al., 2022). The Weather Research and Forecasting model with Chemistry,
226 which theoretically takes these factors into account, was used to simulate the isoprene
227 concentrations. However, substantial divergences were noted between the simulated
228 and observed values at hourly or even daily resolution (Figure S3), demonstrating the
229 challenge for chemical transport models in accurately simulating isoprene (Morichetti
230 et al., 2022; Wang et al., 2024b).

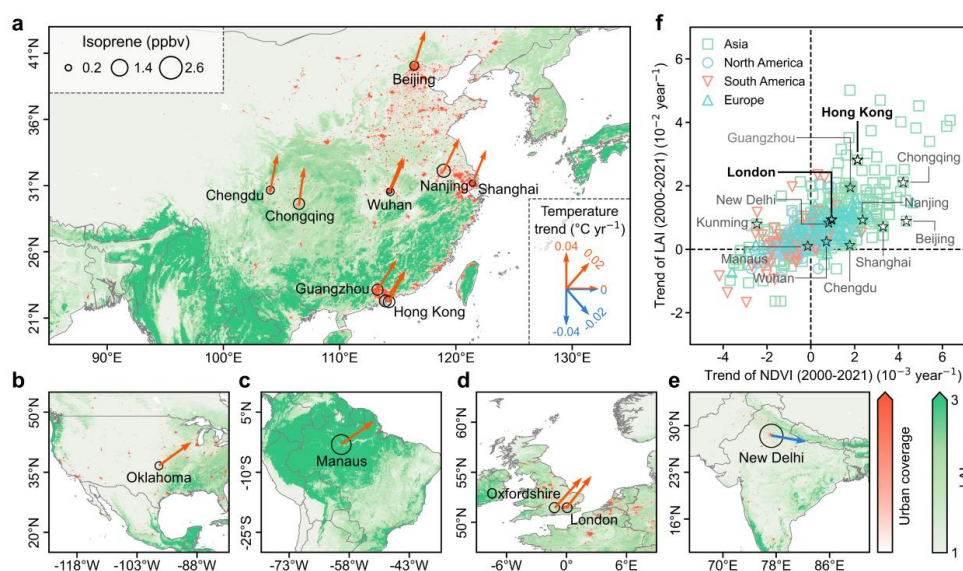


Figure 1. Geographical distribution of the isoprene sampling sites. (a-e) Locations of isoprene measurement sites in China (a), North America (b), Amazonia (c), United Kingdom (d), and India (e). The direction of arrows represents the trend of temperature from 1990 to 2023, and the size of the circle is proportional to isoprene concentration. (f) Trends of LAI and NDVI from 2001 to 2021 in major cities around the world.

We then examined the isoprene prediction ability of various machine learning algorithms with three training strategies: T, NT, and MIX (see Section 2.3). Overall, the model utilizing the NT training strategy exhibited higher fitting accuracy than the one employing the MIX training strategy (Figure 2). This suggests that training with data from different sites might introduce additional noises, due to the differences in isoprene emission dynamics. Particularly, isoprene emissions are highly sensitive to local vegetation profiles. While the ResMLP model with the NT training strategy (ResMLP_{NT}) performed moderately among all the algorithms, the performance was improved by incorporating the T strategy. Specifically, the ResMLP_T outperformed the other algorithms at 8 out of 10 sites, with the decrease in NMAE of 1%–5% and increase in R^2 of 0.01–0.07. The results indicated that the ResMLP_T model effectively exploited the implicit prior knowledge from the pre-training data to guide isoprene prediction at the target sites. Importantly, the pre-trained parameters were fine-tuned using limited



250 sizes of local data, which adapted the model to local isoprene emission dynamics
251 without requiring region-specific vegetation profiles, such as vegetation types and
252 corresponding emission factors. It is worth noting that the size of the retraining data at
253 the validation sites was ~30% of all the data. Thus, the model's good performance at
254 the validation sites demonstrated its utility in data-scarce regions. Furthermore, with
255 the incorporation of PINN, the PINN-ResMLP_T showed a better understanding of the
256 real target-feature relationships with more interpretable prediction results. The model
257 performance was further improved, as indicated by the highest R^2 values across all the
258 sites (Figure 2).

259 Next, we also validated the PINN-ResMLP_T model by applying it to predict isoprene
260 concentrations at the overseas sites (Figure 1). The model was pre-trained with the
261 complete dataset from all the sites in China, which was further fine-tuned with 70% of
262 the data at the individual target sites and validated with the remaining data. Compared
263 to the suboptimal model, the PINN-ResMLP_T model significantly improved the
264 prediction of isoprene, especially at New Delhi and Manaus, with the increase in R^2
265 (decrease by NMAE) by 0.07 (25%) and 0.08 (13%), respectively (Figure 2). This
266 demonstrated the model's broad applicability. Moreover, the model outperforms many
267 other methods in predicting isoprene. For instance, the root mean square error of the
268 PINN-ResMLP_T at Manaus was 0.17 ppbv, compared to 0.95 ppbv for the early attempt
269 in Cross-track Infrared Sounder retrieval (Fu et al., 2019). This superior performance
270 establishes the PINN-ResMLP_T as our best choice. In fact, we would expect more
271 accurate predictions if the model were pre-trained by a wider range of field
272 measurement data from various regions.

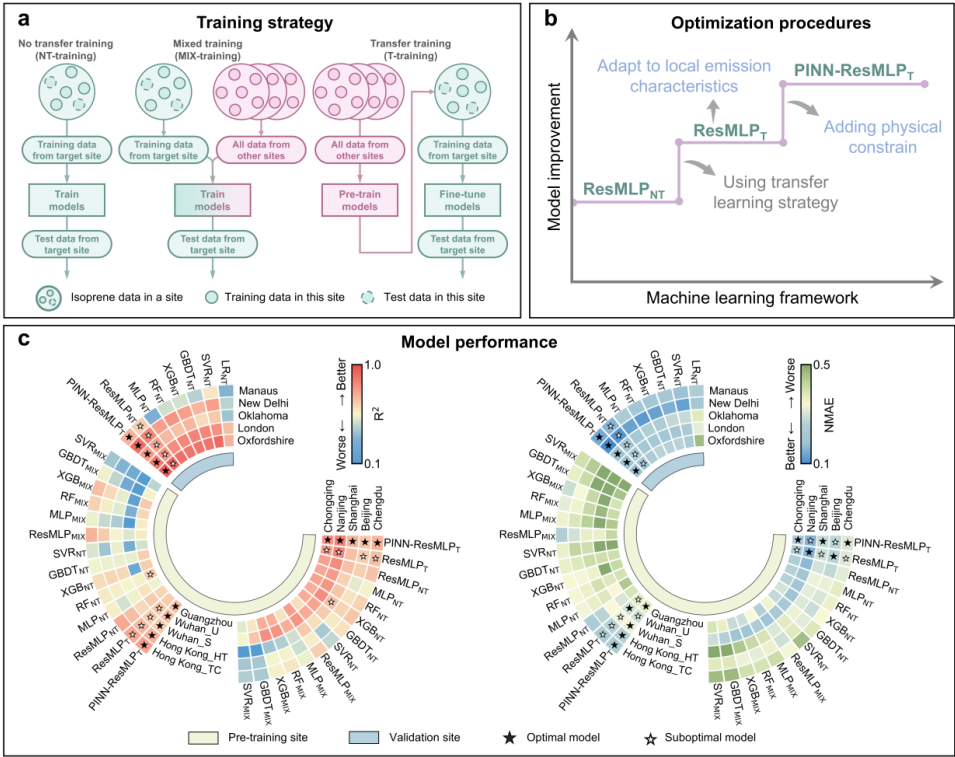


Figure 2. Schematic of the machine learning framework for predicting isoprene concentration. (a) A sketch of the training strategy. (b) The improvement of the machine learning framework. (c) Comparisons of statistical performance across different algorithms in individual sites. See methods for the full names of the algorithms.



279 3.2 Main Factors Influencing Urban Isoprene Concentrations

280 Further, a feature importance method based on the the SHapley Additive exPlanations
281 (SHAP) values was employed to explore the prediction results (Figure 3). While we
282 prefer to present it for individual sites, the feature importance of VI and BC_{traffic} was
283 not calculated for the Chinese sites except a suburban site in Hong Kong (HK_TC), due
284 to the low temporal resolutions of VI and BC_{traffic} data and the short isoprene
285 observation periods. Here, we discuss the drivers of short-term (2-4 years) and long-
286 term (over 10 years) isoprene concentration variations, separately.

287 With the VI and BC_{traffic} remaining relatively stable in the short term, the model
288 indicated that temperature, radiation, surface pressure, and soil water vapor were the
289 most significant drivers of short-term isoprene variations, and their average relative
290 importance was 18.8%, 11.9%, 11.3%, and 8.1% across the all the Mainland China sites,
291 respectively. In addition, evaporation from vegetation transpiration and relative
292 humidity also played significant roles in affecting isoprene concentrations at the Wuhan
293 suburban site and Beijing urban site, respectively. The model also effectively captured
294 the target-feature relationships. In China, the predicted isoprene concentrations
295 increased with temperature below ~35 °C, above which a decline occurred at some sites.
296 A typical example was the response in Chongqing with frequent occurrence of high
297 temperature extremes (Figure S4). High temperatures suppress vegetation emissions
298 due to a reduction in enzyme activity and substrate availability while accelerating the
299 photochemical oxidation loss of isoprene. A similar pattern was observed in the
300 response of isoprene concentrations to radiation in China, especially at extremely high
301 levels. Such nonlinear responses are critical to the parameterization of isoprene
302 emissions in numerical models. Notably, recent studies have revealed substantial
303 uncertainties in the MEGAN model's performance under extreme heat conditions
304 (Wang et al., 2024a). In contrast, our data-driven machine learning approach effectively
305 captures these complex, nonlinear relationships between isoprene concentrations and
306 environmental predictors, offering a promising pathway to refine and optimize
307 parameterization schemes in chemical transport models. In addition to the close



relationships with temperature, solar radiation affects the hydroxyl radical concentrations and therefore can significantly increase chemical loss of isoprene. In contrast, these phenomena were not observed in London, because of lower temperatures and weaker solar radiations. Overall, our transfer learning model reasonably reflected the isoprene-meteorology relationships.

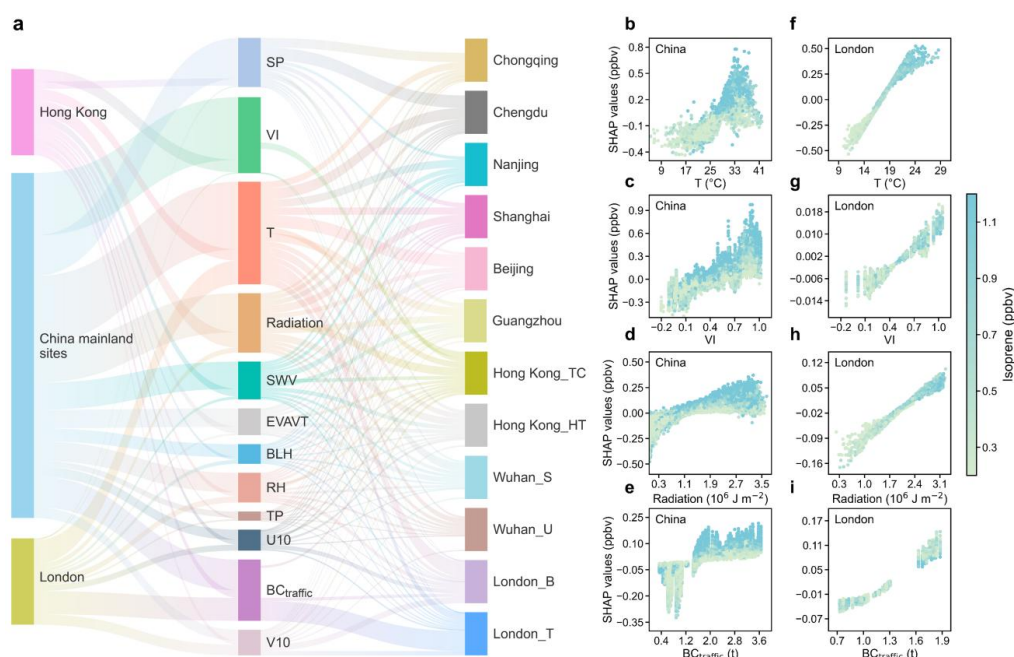


Figure 3. Modeling explainable results at each site based on SHAP value. (a) Feature importance for isoprene concentrations at individual sites. (b-i) The SHAP dependence plots of major influencing variables averaged at the Chinese sites (b-e) and London sites (f-i).

Further, the long-term isoprene observations in London and Hong Kong offer an opportunity to examine how the evolutions of VI and BC_{traffic} affected isoprene variations on a climatic scale. As two prominent international cities, London and Hong Kong are characterized by distinct climatic zones: London experiences a mid-latitude temperate maritime climate, whereas Hong Kong is influenced by a low-latitude subtropical monsoon climate. This climatic differentiation is reflected in their predominant vegetation types, with temperate deciduous trees being prevalent in



324 London and evergreen broad-leaved trees dominating the landscape in Hong Kong.
325 Furthermore, the trajectories of urbanization and air pollution management have
326 evolved differently in each city, shaped by their unique environmental and socio-
327 economic contexts. Here, we focus on the results at two London sites and a Hong Kong
328 site, where long term data was available. Radiation, VI and temperature were the most
329 predominant influencing factors at the suburban site in Hong Kong. In contrast, the
330 relative importance of VI was low at the two London sites. Over the period of 2000–
331 2021, Hong Kong has experienced a notable increase in NDVI ($2.1 \times 10^{-3} \text{ year}^{-1}$) and
332 LAI ($2.8 \times 10^{-2} \text{ year}^{-1}$), while the rate was much lower in London, i.e., $0.9 \times 10^{-3} \text{ year}^{-1}$
333 for NDVI and $0.9 \times 10^{-2} \text{ year}^{-1}$ for LAI. Additionally, the significant difference in VI
334 importance between Hong Kong and London might also be attributed to the different
335 strength of vegetation emissions across latitudes (Guenther et al., 2006; Guenther et al.,
336 2012). Instead, $\text{BC}_{\text{traffic}}$ (temperature) ranked the first at the traffic (suburban) site in
337 London, followed by other meteorological factors (Figure 3). While the meteorological
338 impacts were not surprising, isoprene correlated well with the $\text{BC}_{\text{traffic}}$ emissions and
339 observed benzene at the London traffic site (Figure S5), thereby the high relative
340 importance of $\text{BC}_{\text{traffic}}$. This is consistent with the previous studies on traffic emissions
341 of isoprene in London (Borbon et al., 2001; Von Schneidemesser et al., 2011). As
342 constrained using the PINN, the SHAP values for isoprene concentrations of VI and
343 $\text{BC}_{\text{traffic}}$ showed a monotonic increasing trend.

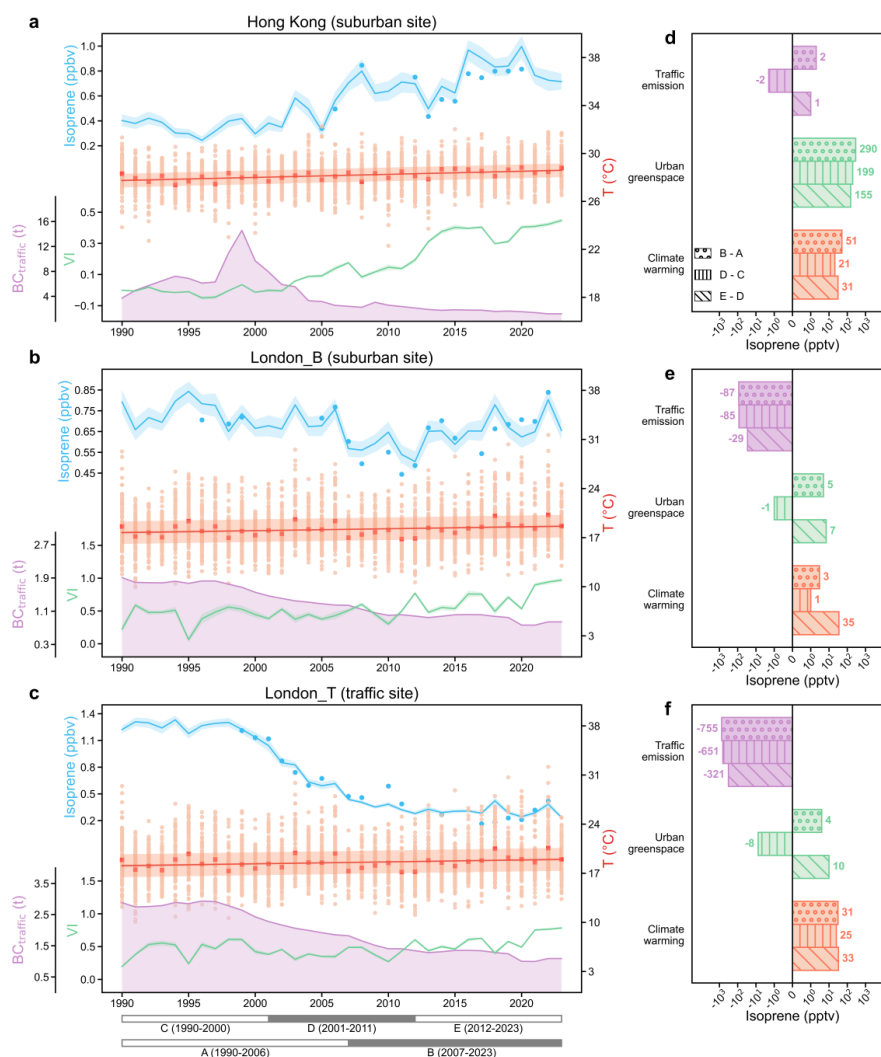
344



345 **3.3 Factors Driving Long-term Trends of Isoprene**

346 The model was also used to build the time series data of daytime isoprene
347 concentrations at a daily resolution over a climatically relevant period (1990–2023) at
348 the three sites with long-term but incomplete isoprene data. The comparison between
349 the geographically distinctive London and Hong Kong offers a rare opportunity to
350 examine the different drivers of isoprene trends. As shown in Figure 4, the predicted
351 isoprene concentrations were in good agreement with the observations, with the R^2 of
352 0.68–0.83 and NMAE of 21%–27%. It's worth noting that the observational data was
353 missing for 50%–67% of the dates at the three sites. This underscored the model's
354 effectiveness in retrieving historical isoprene concentrations from limited observation
355 data.

356 Over the past 34 years, the isoprene concentrations at the Hong Kong site have shown
357 an increasing trend with the rate of 18.1 pptv year⁻¹, as have the temperature and VI. In
358 contrast, traffic emissions have been significantly reduced since 1998, due to the
359 effective human interventions. The trend of the predicted isoprene correlated strongly
360 with the SHAP values of VI ($R = 0.95$) and moderately with that of temperature ($R =$
361 0.63). By fixing the variables one by one, we determined the variations in factor
362 contributions to isoprene concentrations, which were then compared between different
363 time periods. It was found that urban greenspace emerged as the dominant factor
364 impacting Hong Kong's isoprene levels, causing a rise in isoprene concentrations of
365 290 pptv between the last 17 years and the first 17 years. Meanwhile, the contribution
366 of climate warming was 51 pptv, while the traffic contribution was minor. Moreover,
367 without changes in urban greenspace, the coefficient of variation (CV) of annual
368 average isoprene concentrations would decrease by 70.5%, in comparison to the
369 decrease of 12.0% and 6.0% in absence of changes in climate warming and traffic
370 emissions, respectively. This reiterated the significant impacts of urban greenspace on
371 the variations and trends of isoprene concentrations.



372

373 **Figure 4.** Long-term trends of the summertime isoprene and the drivers. **(a-c)** Variations of
 374 isoprene concentrations (blue lines for simulated, blue dots for observed), temperature (T),
 375 urban greenspace (VI) and traffic emissions (BC_{traffic}) in Hong Kong **(a)** and London **(b and c)**.
 376 The red dots and red line represent temperature and the fitted trend for the mean temperature,
 377 respectively. The bands represent 95% confidence intervals. **(d-f)** Changes in isoprene
 378 concentrations caused by climate warming, urban greenspace and traffic emissions in Hong
 379 Kong **(d)** and London **(e and f)** during different periods.



380 In contrast, the isoprene concentrations in London were lower in the last 17 years.
 381 Climate warming would have increased the isoprene concentrations by 31 pptv
 382 compared to those in the first 17 years at the traffic site, while the impact at the suburban
 383 site and the effects of urban greenspace at both sites were negligible. Interestingly,
 384 traffic emissions accounted for 87 pptv and 755 pptv of isoprene reduction at the
 385 suburban site and the traffic site, respectively. This was likely attributed to stringent
 386 traffic emission controls, as indicated by the significant downward trend of BC_{traffic} .
 387 The effect was more pronounced during the first two thirds of the study period (1990–
 388 2011). Specifically, the traffic-related isoprene reduction was 85 pptv from the first
 389 (1990–2000) to the second decade (2001–2011) at the suburban site, in comparison to
 390 the 29 pptv between the second and the last decade (2012–2023). Actually, the observed
 391 isoprene concentration correlated moderately ($R = 0.60$) with BC_{traffic} from 1990 to
 392 2011 based on their annual averages. This suggests that traffic emission controls also
 393 affected isoprene concentrations even in non-urban areas. Despite the higher VI in
 394 London, the increasing rate (1.2 year^{-1} at the suburban site and 0.7 year^{-1} at the traffic
 395 site) was lower than that in Hong Kong (1.6 year^{-1}). Additionally, the weak effects of
 396 urban greenspace might be also due to the relatively low emission strengths of high-
 397 latitude vegetation (Guenther et al., 2006). Moreover, the impact of climate warming
 398 became evident in the last decade (2012–2023) at the suburban site in London and,
 399 together with urban greenspace, reversed the isoprene reduction that would otherwise
 400 have been achieved by traffic emission controls. This aligned with the accelerated
 401 temperature rise from 2011 onwards (Figure S6), which was also reported elsewhere
 402 (Cao et al., 2021). From the perspective of variations in annual isoprene concentrations,
 403 the CV at the traffic site primarily resulted from changes in traffic emissions. At the
 404 suburban site, it would decrease by 32.4% and 14.0% if temperature and traffic
 405 emissions did not change.

406 Overall, our results demonstrate a tale of two cities: similarities and differences in
 407 drivers of long-term isoprene trends. Temperature-driven increases in isoprene
 408 concentrations were revealed in both cities, especially in the last decade, underscoring



409 the universal impacts of climate warming on vegetation emissions. However, the
410 disparities in green space changes and probably different biogenic isoprene emission
411 strengths between the two cities led to the different effects of VI on isoprene variations.
412 Additionally, the isoprene variations over the 34 years have been more influenced by
413 traffic emissions in London, although both cities have implemented stringent vehicle
414 emission controls. While the reasons remain to be explored, we did not identify any
415 correlation between the observed isoprene and BC_{traffic} (or benzene) in Hong Kong,
416 even at a traffic site (Figure S5).

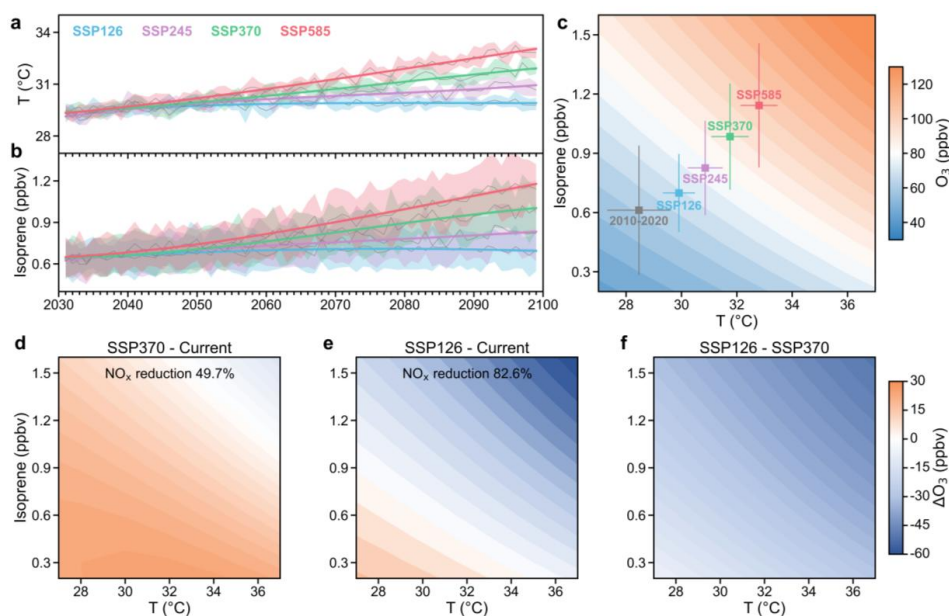
417



418 **3.4 Future Projections for Isoprene and O₃**

419 A significant issue associated with increasing isoprene levels in a warming climate is
 420 the potential for elevated ground-level O₃ pollution. We used the temperature from the
 421 latest CMIP6 multi-model ensemble forecasts to predict isoprene concentrations from
 422 2030 to 2100 in Hong Kong under four IPCC's shared socio-economic pathway (SSP)
 423 scenarios, while the other factors were kept constant. As shown in Figure 5a, the
 424 temperature is expected to increase by 0.71–3.60 °C from 2030 to 2100. The model
 425 indicated that the daytime average concentration of isoprene would increase by 87–530
 426 pptv (15%–87%) by 2100 (Figure 5b). The changes are on the same magnitude as the
 427 previous estimates that isoprene emissions will increase by 21%–57% by the end of this
 428 century relative to the 1990–2010 levels (Cao et al., 2021; Sanderson et al., 2003).

429 Further, we simulated the O₃-isoprene-temperature relationships in Hong Kong (as an
 430 example) using future temperatures and isoprene concentrations while fixing the other
 431 air pollutants and meteorological conditions at present levels. The simulated O₃
 432 increased markedly with the rise in temperature and isoprene concentrations (Figure
 433 5c-5f). The O₃ concentration would increase by up to 1.7 folds by 2100 under the
 434 SSP585 scenario of temperatures and isoprene. An increase in the combined risk of heat
 435 and O₃ exposure could be expected. To explore the approach of alleviating the adverse
 436 impact of O₃-isoprene-temperature synergy, we proposed additional scenarios by
 437 cutting anthropogenic NO_x emissions. With the NO_x reduction from the current to
 438 different SSPs levels, the O₃ concentrations would increase and decrease under low and
 439 high isoprene-temperature conditions, respectively (Figure 5d-5f). This inconsistent
 440 variation is due to the evolution of O₃ formation regime with the rising temperatures
 441 and isoprene. It is worth noting that more ambitious NO_x reduction would result in
 442 greater O₃ benefits. For example, O₃ would decrease in a much wider range of
 443 temperature and isoprene when NO_x is reduced under SSP126. The O₃ growth by 2100
 444 would be only 1.2 folds in the SSP585 scenario of temperatures and isoprene. Therefore,
 445 substantial reduction in anthropogenic NO_x would effectively address the synergy
 446 between temperature, isoprene and O₃.



447

Figure 5. Projected temperature, isoprene and O₃-isoprene-temperature relationships under different climate scenarios. **(a-b)** Projections of the summertime daytime air temperature **(a)** and isoprene concentrations **(b)** during 2030-2100 in Hong Kong. The shaded areas represent the 25th to 75th percentile of the estimated isoprene concentration and temperature for each SSP. **(c-f)** Responses of simulated O₃ concentrations to temperature and isoprene under abundant-NO_x **(c)** and reduced-NO_x **(d-f)** conditions. The squares represent the projected O₃ concentrations at specific temperatures and isoprene levels, with error bars indicating the standard deviation of isoprene concentrations and temperatures.

456



457 **4 Conclusions**

458 As one of the most reactive and abundant VOC, isoprene plays a significant role in
459 shaping urban air quality. We developed an explainable deep transfer learning
460 framework to predict isoprene concentrations and elucidate the underlying drivers of
461 their variability. Our model outperformed conventional approaches, effectively
462 capturing the spatial heterogeneity of isoprene concentrations through localized fine-
463 tuning. Leveraging this framework, we quantified the relative importance of factors
464 influencing isoprene concentrations across numerous sites in China and internationally.
465 The contrasting cases of Hong Kong and London highlight how isoprene dynamics
466 were shaped by distinct local drivers, underscoring the need to tailor air quality
467 management strategies to specific urban contexts. Despite the anticipated increase in
468 biogenic emissions in a warming climate, our findings caution against reducing urban
469 greenspace solely based on isoprene-related concerns. Instead, mitigating global
470 warming emerges as a crucial strategy for managing isoprene's air quality impacts, as
471 evidenced by the strong isoprene–temperature relationships observed. For O₃
472 abatement, coordinated control of NO_x emissions appears effective in reducing the
473 contribution of isoprene to O₃ formation. Moreover, the differing responses of isoprene
474 to VI between Hong Kong and London suggest that informed tree species selection can
475 serve as an alternative urban planning measure. Traffic emissions may also remain a
476 significant source of urban isoprene in cities lacking stringent vehicle emission controls
477 and should be addressed accordingly. Overall, this study provides novel insights into
478 isoprene emissions and chemistry, air quality impacts, and practical mitigation
479 strategies. Nonetheless, limitations persist, particularly regarding the comprehensive
480 representation of emissions and chemical loss processes, which are discussed in Text
481 S2.

482



483 **Acknowledgments**

484 This work was supported by National Key Research and Development Program
485 (2023YFC3709304), Hong Kong Research Grants Council via the General Research
486 Fund (HKBU 15219621, HKBU 15209223), National Natural Science Foundation of
487 China (42575120, 42293322), Public Policy Research Funding Scheme
488 (2023.A2.059.23C), the Youth Fund Project of the Sichuan Provincial Natural Science
489 Foundation (24NSFSC2988), and the Fundamental Research Funds for the Central
490 Universities (YJ202313).

491 **Open Research**

492 Meteorology data for 1990-2023 at each site were obtained from the hourly ERA5
493 reanalysis dataset (Hersbach et al., 2023); The CMIP6 model outputs can be accessed
494 at <https://pcmdi.llnl.gov/CMIP6/>; The NDVI data from 1990-2022 are available at
495 <https://doi.org/10.3334/ORNLDAAAC/2187>; The GLASS LAI V5 and V6 products are
496 downloaded from <https://www.glass.hku.hk/download.html> and
497 <https://www.geodata.cn/main/>, respectively.

498 **Author contributions**

499 X.L. and N.W. conceived the study. S.L. developed the methodology. Data collection
500 was performed by S.L., N.W., X.L., Z.S., X.H., T.L., H.W., M.L., J.G., N.C., G.S., Y.Z.,
501 C.P., Z.L., C.T., and X.L. Data analysis was conducted by S.L., X.L., and N.W. N.W.
502 and X.L. led the investigation and supervision. Visualization was completed by S.L.
503 and N.W. The original draft was written by S.L., N.W., and X.L. All authors, including
504 F.Y., Z.S., X.H., and A.G., contributed to reviewing and editing the manuscript.

505 **Competing Interests**

506 The authors declare that they have no known competing financial interests or personal
507 relationships that could have appeared to influence the work.

508

509



510 **Reference**

- 511 Arneth, A., Schurgers, G., Lathiere, J., et al.: Global terrestrial isoprene emission
 512 models: sensitivity to variability in climate and vegetation, *Atmos. Chem. Phys.*, 11,
 513 8037-8052, 10.5194/acp-11-8037-2011, 2011.
- 514 Borbon, A., Fontaine, H., Veillerot, M., et al.: An investigation into the traffic-related
 515 fraction of isoprene at an urban location, *Atmos. Environ.*, 35, 3749-3760,
 516 [https://doi.org/10.1016/S1352-2310\(01\)00170-4](https://doi.org/10.1016/S1352-2310(01)00170-4), 2001.
- 517 Cao, Y., Yue, X., Liao, H., et al.: Ensemble projection of global isoprene emissions by
 518 the end of 21st century using CMIP6 models, *Atmos. Environ.*, 267, 118766,
 519 <https://doi.org/10.1016/j.atmosenv.2021.118766>, 2021.
- 520 Fu, D., Millet, D. B., Wells, K. C., et al.: Direct retrieval of isoprene from satellite-
 521 based infrared measurements, *Nat. Commun.*, 10, 3811, 10.1038/s41467-019-11835-0,
 522 2019.
- 523 Guenther, A., Zimmerman, P., and Wildermuth, M.: Natural volatile organic compound
 524 emission rate estimates for U.S. woodland landscapes, *Atmos. Environ.*, 28, 1197-1210,
 525 [https://doi.org/10.1016/1352-2310\(94\)90297-6](https://doi.org/10.1016/1352-2310(94)90297-6), 1994.
- 526 Guenther, A., Karl, T., Harley, P., et al.: Estimates of global terrestrial isoprene
 527 emissions using MEGAN (Model of Emissions of Gases and Aerosols from Nature),
 528 *Atmos. Chem. Phys.*, 6, 3181-3210, 10.5194/acp-6-3181-2006, 2006.
- 529 Guenther, A. B., Zimmerman, P. R., Harley, P. C., et al.: Isoprene and monoterpene
 530 emission rate variability: Model evaluations and sensitivity analyses, *J. Geophys. Res.-*
 531 *Atmos.*, 98, 12609-12617, <https://doi.org/10.1029/93JD00527>, 1993.
- 532 Guenther, A. B., Jiang, X., Heald, C. L., et al.: The Model of Emissions of Gases and
 533 Aerosols from Nature version 2.1 (MEGAN2.1): an extended and updated framework
 534 for modeling biogenic emissions, *Geosci. Model Dev.*, 5, 1471-1492, 10.5194/gmd-5-
 535 1471-2012, 2012.
- 536 Hersbach, H., Bell, B., Berrisford, P., Biavati, G., Horányi, A., Muñoz Sabater, J.,
 537 Nicolas, J., Peubey, C., Radu, R., Rozum, I., & Schepers, D. (2023). ERA5 hourly
 538 data on single levels from 1940 to present [Dataset]. European Centre for Medium-
 539 Range Weather Forecasts (ECMWF). <https://doi.org/10.24381/cds.adbb2d47>.



540 Huang, G., Brook, R., Crippa, M., et al.: Speciation of anthropogenic emissions of non-
541 methane volatile organic compounds: a global gridded data set for 1970–2012, *Atmos.*
542 *Chem. Phys.*, 17, 7683–7701, 10.5194/acp-17-7683-2017, 2017.

543 Li, M., Huang, X., Yan, D., et al.: Coping with the concurrent heatwaves and ozone
544 extremes in China under a warming climate, *Sci. Bull.*,
545 <https://doi.org/10.1016/j.scib.2024.05.034>, 2024.

546 Lin, Y.-H., Zhang, H., Pye, H. O. T., et al.: Epoxide as a precursor to secondary organic
547 aerosol formation from isoprene photooxidation in the presence of nitrogen oxides,
548 *Proc. Natl. Acad. Sci. U. S. A.*, 110, 6718–6723, doi:10.1073/pnas.1221150110, 2013.

549 Lyu, X., Li, H., Lee, S.-C., et al.: Significant Biogenic Source of Oxygenated Volatile
550 Organic Compounds and the Impacts on Photochemistry at a Regional Background Site
551 in South China, *Environ. Sci. Technol.*, 58, 20081–20090, 10.1021/acs.est.4c05656,
552 2024.

553 Ma, M., Gao, Y., Wang, Y., et al.: Substantial ozone enhancement over the North China
554 Plain from increased biogenic emissions due to heat waves and land cover in summer
555 2017, *Atmos. Chem. Phys.*, 19, 12195–12207, 10.5194/acp-19-12195-2019, 2019.

556 Ma, M., Gao, Y., Ding, A., et al.: Development and Assessment of a High-Resolution
557 Biogenic Emission Inventory from Urban Green Spaces in China, *Environ. Sci.*
558 *Technol.*, 56, 175–184, 10.1021/acs.est.1c06170, 2022.

559 Morichetti, M., Madronich, S., Passerini, G., et al.: Comparison and evaluation of
560 updates to WRF-Chem (v3.9) biogenic emissions using MEGAN, *Geosci. Model Dev.*,
561 15, 6311–6339, 10.5194/gmd-15-6311-2022, 2022.

562 Paulot, F., Henze, D. K., and Wennberg, P. O.: Impact of the isoprene photochemical
563 cascade on tropical ozone, *Atmos. Chem. Phys.*, 12, 1307–1325, 10.5194/acp-12-1307-
564 2012, 2012.

565 Peron, A., Graus, M., Striednig, M., et al.: Deciphering anthropogenic and biogenic
566 contributions to selected non-methane volatile organic compound emissions in an urban
567 area, *Atmos. Chem. Phys.*, 24, 7063–7083, 10.5194/acp-24-7063-2024, 2024.



568 Pfannerstill, E. Y., Arata, C., Zhu, Q., et al.: Temperature-dependent emissions
 569 dominate aerosol and ozone formation in Los Angeles, *Science*, 384, 1324-1329,
 570 10.1126/science.adg8204, 2024.

571 Sanderson, M. G., Jones, C. D., Collins, W. J., et al.: Effect of Climate Change on
 572 Isoprene Emissions and Surface Ozone Levels, *Geophys. Res. Lett.*, 30,
 573 <https://doi.org/10.1029/2003GL017642>, 2003.

574 Seco, R., Holst, T., Davie-Martin, C. L., et al.: Strong isoprene emission response to
 575 temperature in tundra vegetation, *Proc. Natl. Acad. Sci. U. S. A.*, 119, e2118014119,
 576 doi:10.1073/pnas.2118014119, 2022.

577 Tripathi, N., Sahu, L. K., Wang, L., et al.: Characteristics of VOC Composition at
 578 Urban and Suburban Sites of New Delhi, India in Winter, *J. Geophys. Res.-Atmos.*,
 579 127, e2021JD035342, <https://doi.org/10.1029/2021JD035342>, 2022.

580 von Schneidmesser, E., Monks, P. S., Gros, V., et al.: How important is biogenic
 581 isoprene in an urban environment? A study in London and Paris, *Geophys. Res. Lett.*,
 582 38, <https://doi.org/10.1029/2011GL048647>, 2011.

583 Wang, H., Nagalingam, S., Welch, A. M., et al.: Heat waves may trigger unexpected
 584 surge in aerosol and ozone precursor emissions from sedges in urban landscapes, *Proc.*
 585 *Natl. Acad. Sci. U. S. A.*, 121, e2412817121, 10.1073/pnas.2412817121, 2024a.

586 Wang, H., Welch, A. M., Nagalingam, S., et al.: High temperature sensitivity of Arctic
 587 isoprene emissions explained by sedges, *Nat. Commun.*, 15, 6144, 10.1038/s41467-
 588 024-49960-0, 2024b.

589 Xu, L., Guo, H., Boyd, C. M., et al.: Effects of anthropogenic emissions on aerosol
 590 formation from isoprene and monoterpenes in the southeastern United States,
 591 *Proceedings of the National Academy of Sciences*, 112, 37-42,
 592 10.1073/pnas.1417609112, 2015.

593 Xu, P., Li, G., Zheng, Y., et al.: Fertilizer management for global ammonia emission
 594 reduction, *Nature*, 626, 792-798, 10.1038/s41586-024-07020-z, 2024.

595

596